Applied Acoustics 103 (2016) 90–101

Contents lists available at ScienceDirect

Applied Acoustics

journal homepage: www.elsevier.com/locate/apacoust

Hybrid smoothed finite element method for two dimensional acoustic radiation problems

Y.B. Chai [a], W. Li [a,b,c,*], Z.X. Gong [a], T.Y. Li [a,b,c]

[a] School of Naval Architecture and Ocean Engineering, Huazhong University of Science and Technology, Wuhan, Hubei 430074, China
[b] Hubei Key Laboratory of Naval Architecture & Ocean Engineering Hydrodynamics (HUST), Wuhan, Hubei 430074, China
[c] Collaborative Innovation Center for Advanced Ship and Deep-Sea Exploration (CISSE), Shanghai 200240, China

ARTICLE INFO

Article history:
Received 8 May 2015
Received in revised form 6 October 2015
Accepted 14 October 2015
Available online 29 October 2015

Keywords:
Hybrid smoothed finite element method (HS-FEM)
Dirichlet-to-Neumann (DtN) condition
Acoustic radiation
Dispersion error
Numerical methods

ABSTRACT

It is well known that one key difficulty of solving the boundary-value problems governed by the Helmholtz equation using standard finite element method (FEM) is the loss of accuracy with increasing wave number due to the "numerical dispersion error". In order to overcome this issue, the hybrid smoothed finite element method (HS-FEM) using linear triangular elements is presented to analyze two dimensional radiation problems. An important feature of HS-FEM is the introduction of a scale factor $\alpha \in [0, 1]$ which is designed to establish the area-weighted strain field that contains contributions from both the standard FEM and the node-based smoothed finite element method (NS-FEM). The gradient smoothing technique used in the HS-FEM guarantees the numerical model can provide a close-to-exact stiffness to the continuous system and hence significantly reduces the numerical dispersion error. To solve the acoustic radiation problems in an infinite fluid domain, the HS-FEM is combined with the Dirichlet-to-Neumann (DtN) boundary condition to give a HS-FEM-DtN model for two dimensional acoustic radiation problems. Several numerical examples are given and it is found that HS-FEM can provide more accurate results than FEM with the same mesh.

1. Introduction

During the past few decades, a variety of numerical methods have been introduced to solve acoustic problems governed by the Helmholtz equation. The standard finite element method (FEM) and boundary element method (BEM) are the most popular and powerful numerical methods for coping with these acoustic problems. There are a great deal of relevant research work can be found in the published literatures [1–5]. However, the numerical approaches for handling the acoustic problems still remain two major challenges. In general, the acoustic problems can be classified into interior and exterior acoustic problems. The first challenge is how to treat exterior acoustic problems in an infinite fluid domain effectively. Initially, the FEM was applied to acoustics with the aim of solving the interior problems in finite domains. For exterior problems, including acoustic radiation and scattering, the well-known Sommerfeld radiation condition should be obeyed so that there is no spurious wave reflecting from the far field. Another challenge is the so-called "numerical dispersion" errors [6–8]. In general, the numerical methods can provide appropriate solutions in the low frequency range (small wave number). While the accuracy of the numerical solutions will deteriorate rapidly as the wave number is increased. A simple way of improving the accuracy of numerical solutions is to employ high quality meshes. However, refining the mesh may become prohibitively expensive. This difficulty is especially important when solving large-scale 3D acoustic problems, and hence it is not always a viable option.

Actually, standard FEM is not appropriate for solving exterior acoustic problems in infinite domains. To remedy this difficulty, a series of numerical treatments including absorbing boundary conditions [9–12], Dirichlet to Neumann (DtN) boundary conditions [13–17] and perfectly matched layer (PML) [18–20] have been introduced to deal with exterior acoustic problems in recent years. One outstanding numerical technique of them is the DtN boundary condition devised by Givoli and Keller. This boundary condition is an exact non-reflecting boundary condition (there are no spurious reflecting waves from far field) and it relates the "Dirichlet datum" to the "Neumann datum" with the help of an integral operator *M*. Even though it is non-local, it still possesses high computational efficiency and can obtain much more accurate results than those obtained from various approximate local condi-

* Corresponding author at: School of Naval Architecture and Ocean Engineering, Huazhong University of Science and Technology, Wuhan, Hubei 430074, China.
E-mail address: hustliw@hust.edu.cn (W. Li).

http://dx.doi.org/10.1016/j.apacoust.2015.10.012
0003-682X/

tions. Therefore, many researchers have applied the DtN boundary conditions to cope with all kinds of exterior acoustic problems and other problems in large finite domains.

Grote and Kirsch employed the DtN boundary condition to analyze the time harmonic multiple scattering problems where the computational regions contained several disjoint components [15]. Due to each sub-scatter was enclosed by a separate artificial boundary, the computational efficiency was greatly improved. Acosta and Villamizar proposed a hybrid method employing the DtN boundary condition along with the finite difference method in curvilinear coordinates for the analysis of multiple scattering problems from obstacle of arbitrary shape [21]. In this work, a heterogenous medium with variable physical properties in the vicinity of the obstacles was considered. As an extension of this work, the multiple DtN boundary condition coupling with the method of images was developed for multiple scattering problems in the half-plane [22]. Following Keller, Giboli and Grote's work, a new exact non-reflecting boundary condition on general domains was formulated by Nicholls and Nigam [23]. An important feature of this work was the artificial boundary need not be quite specific, such as a circle in two dimensions or a sphere in three dimensions. The shape of the artificial boundary mainly depended on the shape of the scatters. Numerical results showed that this method not only can obtain accurate solutions, but also enable significant computational savings.

For the purpose of reducing the numerical dispersion error in acoustic problems, various numerical techniques based on the standard finite element method have been developed to tackle this issue, such as the Galerkin/least-squares finite element method (GLS) [24], the quasi-stabilized finite element method (QSFEM) [8] and the residual-free finite element method (RFEM) [25]. However, all of the above methods can not reduce the numerical dispersion error effectively.

In addition to the standard finite element method and the extended finite element method, the meshfree methods have been also introduced to solve the acoustic problems. Belytschko et al. proposed the element-free Galerkin method (EFGM) to tackle the numerical dispersion in acoustic problems [26]. Bouillard and Suleaub [27] found that the EFGM was effective to reduce the numerical dispersion error significantly compared to the FEM even though the EFGM also suffered from the dispersion and pollution effect. However, in order to control the numerical dispersion error, delicate background cells and a large number of quadrature points were needed for the global numerical integration, leading to prohibitive computational demands. The discontinuous finite element formulation has also been applied for acoustic problems by Alvarez et al. and significant improvement were achieved on accuracy, but higher cost in computation as well as EFGM [28].

As mentioned in Ref. [29], the approximate discrete model is the main reason to cause dispersion error. The stiffness of the discretized model obtained from the standard FEM always behaves stiffer than the original model, leading to the so-called numerical dispersion error. So producing a properly "softened" stiffness for the discrete model is much more essential to control the numerical error.

In the advanced finite element method field, a series of smoothed finite element (S-FEM), named as node-based S-FEM (NS-FEM), edge-based S-FEM (ES-FEM) and face-based S-FEM (FS-FEM) was proposed by Liu's group [30–33]. Due to the gradient smoothing technique used in the S-FEM, these S-FEM models can provide proper softening effect to the "overly-stiff" FEM model, the S-FEM shows great efficiency and high convergence rates in solving linear elastic solid mechanics. In recent years, He et al. have introduced the S-FEM to solve the acoustic problems and coupled structural-acoustic problems [34–39]. The linear triangular and tetrahedron elements are used to discretize the 2D and 3D fluid domains. Numerical results demonstrated that the S-FEM is more effective to control the numerical error than the standard FEM.

The present work is inspired by Li and He's work [39] on hybrid smoothed finite element method (HS-FEM) for acoustic problems. The essential idea of the HS-FEM is to introduce a scale factor $\alpha \in [0, 1]$ to establish a continuous function of strain energy that contains contributions from both the standard FEM and the node-based smoothed finite element method (NS-FEM). This novel HS-FEM makes the best use of the "overly-stiff" property of the standard FEM and the "overly-soft" property of the NS-FEM. By regulating the parameter α, the HS-FEM can obtain a "close-to-exact" stiffness of the discretized model and then can provide much more accurate solutions than the standard FEM. While the above mentioned work mainly focus on interior acoustic problems. Our focus in this work is to address the two dimensional radiation problems in unbounded domains which are very important in various scientific fields such as linear and nonlinear wave mechanics. In this paper, the HS-FEM is combined with the DtN boundary condition to give a HS-FEM-DtN model for the exterior acoustic problems. Due to the good performance of the HS-FEM in interior acoustic problems, it is expected that the HS-FEM will solve the exterior acoustic problems with very accurate solutions.

This paper is organized as follows: in Section 2 the acoustic radiation problems in infinite domain is reviewed. Section 3 briefly describes the Dirichlet to Neumann boundary condition for finite element schemes. Section 4 contains the detailed formulation of the hybrid smoothed finite element method. Section 5 outlines the numerical error estimates in acoustic problems. In Section 6, several numerical examples are studied in details. Final conclusions from the numerical results are drawn in Section 7.

2. The acoustic radiation problems in infinite domain

As shown in Fig. 1, an acoustic radiation problem in infinite domain R bounded internally by the surface Γ of an radiator is considered. We assume that the boundary Γ can be decomposed into two portions Γ_p and Γ_v, where $\Gamma = \Gamma_p \cup \Gamma_v$ and $\Gamma_p \cap \Gamma_v = \varnothing$. Γ_p and Γ_v denote the Dirichlet boundary condition and the Neumann boundary condition. The two boundary conditions can be described as follows:

$$p = p_D \quad \text{on} \quad \Gamma_p \tag{1}$$

$$\nabla p \cdot n = -j\rho\omega v_n \quad \text{on} \quad \Gamma_v \tag{2}$$

where p denotes the spatial part of the acoustic pressure or velocity potential, ρ, ω and v_n represent the density of medium, the angular frequency and the normal velocity on the boundary, respectively.

The exterior boundary-value problem can be described in the following equations:

$$\Delta p + k^2 p + f = 0 \quad \text{in} \quad R \tag{3}$$

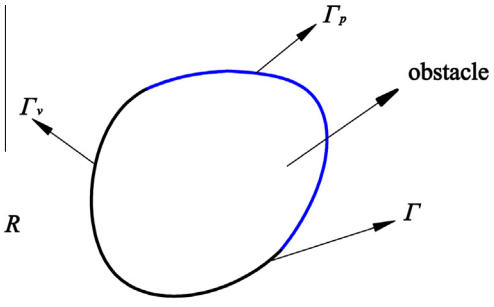

Fig. 1. The acoustic radiation problem in an infinite domain.

$$p = g \quad \text{on} \quad \Gamma_g \tag{4}$$

$$\nabla u \cdot n = h \quad \text{on} \quad \Gamma_h \tag{5}$$

Here, Δ and k represent the Laplace operator and wave number, respectively, f, g and h are given functions.

For acoustic radiation problems in unbounded domains, the Sommerfeld radiation condition has to be obeyed and the radiation condition requires that energy flux be positive at infinity, this property ensures that the boundary-value problem has unique solution.

The Sommerfeld radiation condition can be describe as follows:

$$\lim_{x\to\infty} r^{\frac{(d-1)}{2}}\left(\frac{\partial p}{\partial r} - ikp\right) = 0 \tag{6}$$

where d is the spatial dimension.

3. The formulation of FEM-DtN method

The aim of this paper is to solve two dimensional acoustic radiation problems in infinite domain. In order to solve the exterior Helmholtz equation using numerical method, as shown in Fig. 2, the infinite domain is usually truncated by an artificial boundary B which is generally a circle or sphere of radius R. As a result, a finite computational domain Ω is obtained and the original problem is equivalent to two sub-problems. They are called sub-problem O and sub-problem I.

Sub-problem O in the unbounded domain is the radiation problem of a circle and it is governed by Eqs. (3)–(6). In two dimensions, according to Keller and Givoli [13], the exact solution of this problem can be expressed as:

$$p(r,\theta) = \frac{1}{\pi}{\sum_{n=0}^{\infty}}' \int_0^{2\pi} \frac{H_n^{(1)}(kr)}{H_n^{(1)}(kR)} \cos n(\theta-\theta')p(R,\theta')\mathrm{d}\theta' \tag{7}$$

where $p(r,\theta)$ denotes the unknown value of the acoustic pressure on the inner boundary. The prime after the sum indicates that a factor of 1/2 multiples the term with $n = 0$. $H_n^{(1)}$ represents the Hankel function of the first kind.

Sub-problem I in the bounded domain is the radiation problem of an arbitrary radiator into finite domain the outer of which is a circle. The surface of the radiator is the inner boundary of this problem. As mentioned above, the inner boundary can be divided into two portions, Γ_p and Γ_v. The Dirichlet boundary condition and Neumann boundary condition are imposed on Γ_p and Γ_v, respectively.

The computational domain of sub-problem I is finite and it can be easily solved by the standard finite element method. The governing equation of this problem is given by Eqs. (1)–(3) and a defined boundary condition on the artificial boundary B. the weighted residual equation can be obtained by multiplying Eq. (3) with a test function w. Then integrating over the entire domain and using Green's theorem, the weak form of this problem can be expressed as:

$$\int_\Omega (k^2 wp - \nabla w \cdot \nabla p)d\Omega + \int_B w\frac{\partial p}{\partial n}dB = \int_\Omega fwd\Omega + \int_\Gamma v_n wd\Gamma \tag{8}$$

The second term in Eq. (8), which contains the normal derivative of the acoustic pressure $\frac{\partial p}{\partial n}$ on the artificial boundary is not yet known. Therefore the key to this problem is how to calculate the integral $\int_B w\frac{\partial p}{\partial n}dB$.

One important idea is to find a relation that replaces the normal derivative $\frac{\partial p}{\partial n}$ by the value of p on the artificial boundary. As mentioned in the previous section, sub-problem O can be solved analytically, hence the relation between $\frac{\partial p}{\partial n}$ and p is possible to obtain from the solution of this problem. This is the well-known "Dirich let-to-Neumann" (DtN) condition which relating the Dirichlet datum p to the Neumann datum $\frac{\partial p}{\partial n}$ on the artificial boundary B. The DtN boundary condition can be written in the following form:

$$\frac{\partial p}{\partial n} = -Mp \quad \text{on} \quad B \tag{9}$$

where M denotes the DtN operator.

Once the explicit expressions of the DtN operator M is found, the integration in Eq. (8) can be carried out easily. The normal derivative of the acoustic pressure $\frac{\partial p}{\partial n}$ on the artificial boundary can be obtained from Eq. (7).

$$p_v = \frac{\partial p(r,\theta)}{\partial n}\Big| r = R = -{\sum_{n=0}^{\infty}}' \int_0^{2\pi} m_n(\theta-\theta')p(R,\theta')d\theta' \tag{10}$$

where

$$m_n(\theta-\theta') = -\frac{k}{\pi}\frac{H_n^{(1)}(kR)}{H_n^{(1)}(kR)}\cos n(\theta-\theta') \tag{11}$$

here $m_n(\theta-\theta')$ is the DtN kernels and it can be separated as

$$m_n(\theta-\theta') = -\frac{k}{\pi}\frac{H_n^{(1)}(kR)}{H_n^{(1)}(kR)}(\cos n\theta\cos n\theta' + \sin n\theta \sin n\theta') \tag{12}$$

In this manner, the original problem in infinite domain can be solved successfully. The detained formulation of this problem by finite element method is not given in this paper. Interested readers may refer to Ref. [13]. According to Keller and Givoli, the discretized system equation for this problem can be obtained in the following matrix form:

$$\mathbf{Kp} = \mathbf{F} \tag{13}$$

where $\mathbf{K}$ is the system stiffness matrix, $\mathbf{p}$ is the unknown nodal acoustic pressure in the computational domain, $\mathbf{F}$ is the vector of nodal force.

The system stiffness matrix $\mathbf{K}$ can be written in two parts:

$$\mathbf{K} = \mathbf{K}^a + \mathbf{K}^b \tag{14}$$

where

$$\mathbf{K}^a = [\mathbf{K}_{IJ}^a] \quad \mathbf{K}^b = [\mathbf{K}_{IJ}^b] \tag{15}$$

$$\mathbf{K}_{IJ}^a = a(N_I, N_J) = \int_\Omega (\nabla\mathbf{N})^T\nabla\mathbf{N}d\Omega - k^2\int_\Omega \mathbf{N}^T\mathbf{N}d\Omega \tag{16}$$

$$\mathbf{K}_{IJ}^b = b(N_I, N_J) \tag{17}$$

where $\mathbf{K}^a$ can be derived from the first term of Eq. (8), $\mathbf{K}^b$ contains the DtN boundary condition and can be derived from the second term of Eq. (8), I and J denote the node number and N_I is the defined shape function for node I.

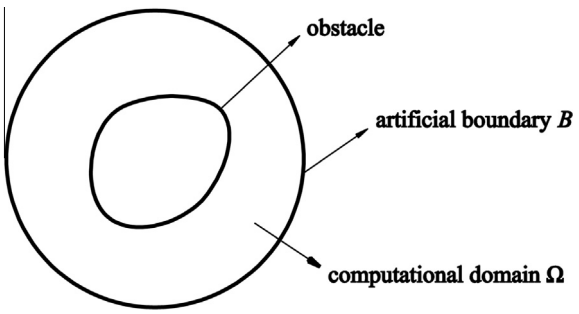

Fig. 2. The infinite domain is usually truncated by an artificial boundary B yielding a finite computational domain Ω.

By substituting Eq. (10) into Eq. (8), the stiffness matrix $\mathbf{K}^b$ which contains the DtN operator M can be obtained as:

$$\mathbf{K}_{IJ}^b = b(N_I, N_J) = \int_B N_I M N_J \mathrm{d}B = -\sum_{j=0}^{\infty} \frac{k}{\pi} \frac{H_n^{(1)}(kr)}{H_n^{(1)}(kR)} \left(\int_B N_I(\mathbf{x}) F_j(\mathbf{x}) \mathrm{d}B \right) \left(\int_B N_J(\mathbf{x}) F_j(\mathbf{x}') \mathrm{d}B \right) \quad (18)$$

where the simple trigonometric functions $F_j(\mathbf{x})$ and $F_j(\mathbf{x}')$ are determined by:

$$F_j(\mathbf{x}) = [\cos n\theta \quad \sin n\theta] \quad (19)$$

$$F_j(\mathbf{x}') = \begin{bmatrix} \cos n\theta' \\ \sin n\theta' \end{bmatrix} \quad (20)$$

It can be seen from Eq. (14) that the effect of the DtN boundary condition on the standard finite element method is the inclusion of the matrix $\mathbf{K}^b$ in the system stiffness $\mathbf{K}$. Due to the local support property of the FEM shape functions, the value of N_I equals 1 at node I and equals 0 at every other node. Besides, N_I will vanish outside a local patch of elements which share node I. Then the matrix $\mathbf{K}_{IJ}^b$ is nonzero only if both nodes I and J lie on the boundary B. The matrix $\mathbf{K}_{IJ}^b$ corresponds to DtN boundary condition, after having calculated $\mathbf{K}_{IJ}^b$, the exterior acoustic problems in unbounded domain can be solved by the standard finite element scheme.

4. Formulation of the hybrid smoothed finite element method (HS-FEM)

4.1. The node-based smoothed finite element method (NS-FEM) for acoustic problems

In the NS-FEM model, the problem domain Ω is first divided into N_e elements with N_n nodes, such that $\Omega = \sum_{i=1}^{N_e} \Omega_i^e$ and $\Omega_i^e \cap \Omega_j^e = \varnothing$, $i \neq j$, as in the standard FEM. The generated elements can be polygons with arbitrary number of sides and used as background elements in the NS-FEM. On the top of the background element mesh, the problem domain Ω is further divided into N_n smoothing domains associated with nodes of the polygonal elements such that $\Omega = \sum_{k=1}^{N_n} \Omega_k^s$ and $\Omega_i^s \cap \Omega_j^s = \varnothing$, $i \neq j$. As shown in Fig. 3, the node-based smoothing domain for node k is created by sequentially connecting the mid-edge-point to the centroids of surrounding n-sided polygonal elements of node k, Γ_k is the boundary of the smoothing domain Ω_k. As a result, the number of the smoothing domain is exactly the same as the number of nodes. Each n-sided polygonal element will be divided into n quadrilateral sub-domains and each sub-domain is attached to the nearest field node. After obtaining the above-mentioned smoothing domains, the node-based smoothing techniques are applied over these smoothing domains to create a continuous strain field for the NS-FEM model. Then the global smoothed acoustic stiffness matrix of NS-FEM can be obtained as:

$$\overline{\mathbf{K}}^{\text{NS-FEM}} = \int_\Omega (\overline{\nabla \mathbf{N}})^T (\nabla \mathbf{N}) \mathrm{d}\Omega = \sum_{k=1}^{N_n} \overline{\mathbf{K}}^{(k)} \quad (21)$$

where $\mathbf{N}$ denotes the FEM shape functions and $\overline{\mathbf{K}}^{(k)}$ is the smoothed element stiffness matrix for node k.

The relation of the acoustic particle velocity v and the acoustic pressure p in ideal fluid can be expressed as:

$$\nabla p + j\rho\omega v = 0 \quad (22)$$

where $j = \sqrt{-1}$, ρ is the density of medium and ω is the angular frequency.

In this present formulation, the acoustic particle velocity field v, which is usually linked to the gradient of acoustic pressure, is smoothed by the node-based smoothing technique and then the smoothed velocity field can be obtained as:

$$\bar{v}(\mathbf{x}_k) = \int_{\Omega_k} v(\mathbf{x}_k) \phi_k(\mathbf{x}) \mathrm{d}\Omega \quad (23)$$

where $\phi_k(\mathbf{x})$ is a given smoothing function that satisfies at least unity property.

$$\int_{\Omega_k} \phi_k(\mathbf{x}) \mathrm{d}\Omega = 1 \quad (24)$$

Using the following constant smoothing function

$$\phi_k(\mathbf{x}) = \begin{cases} 1/A_k & x \in \Omega_k \\ 0 & x \notin \Omega_k \end{cases} \quad (25)$$

where A_k is the area of the smoothing domain for node k.

Substituting Eqs. (22) and (25) into Eq. (23) and using Green's theorem, the smoothed velocity field can be obtained in terms of acoustic pressure.

$$\bar{v}(\mathbf{x}_k) = \frac{1}{A_k} \int_{\Omega_k} v(\mathbf{x}) \phi_k(\mathbf{x}) \mathrm{d}\Omega = -\frac{1}{j\rho\omega A_k} \int_{\Omega_k} \nabla p \mathrm{d}\Omega = -\frac{1}{j\rho\omega A_k} \int_{\Gamma_k} p \cdot n \mathrm{d}\Gamma \quad (26)$$

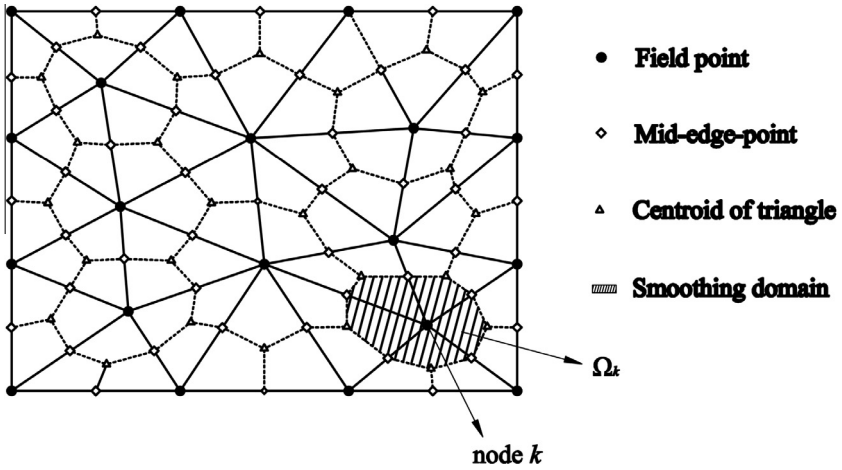

Fig. 3. The node-based smoothing domains in 2D problem are created by sequentially connecting the mid-edge-point to the centroids of surrounding n-sided polygonal elements.

Using the FEM shape functions, the smoothed velocity field can be expressed in the following matrix form:

$$\bar{v}(\mathbf{x}_k) = -\frac{1}{j\rho\omega}\sum_{i\in M_k}\overline{\mathbf{B}}_i(x_k)p_i \tag{27}$$

where M_k is total number of nodes in the influence domain of node k.

$$\overline{\mathbf{B}}_i^T(x_k) = \begin{bmatrix}\bar{b}_{i1} & \bar{b}_{i2}\end{bmatrix} \tag{28}$$

$$\bar{b}_{ip} = \frac{1}{A_k}\int_{\Gamma_k} N_i(x)np(x)\mathrm{d}\Gamma \tag{29}$$

Using Gauss integration scheme along the boundary Γ_k of the smoothing domain Ω_k, the numerical integration in Eq. (29) can be calculated as

$$\bar{b}_{ip} = \frac{1}{A_k}\sum_{q=1}^{N_s}\sum_{r=1}^{N_g} w_r N_i(x_{qr})np(x_q) \tag{30}$$

where N_s is the number of segments of the boundary Γ_k, N_g is the number Gauss points distributed in each segment and w_r is the corresponding weight coefficients for Gauss point.

Then the smoothed element stiffness matrix for smoothing domain Ω_k in Eq. (21) can be obtained as:

$$\overline{\mathbf{K}}^{(k)} = \int_{\Omega_k}\mathbf{B}^T\mathbf{B}d\Omega = \mathbf{B}^T\mathbf{B}A_k \tag{31}$$

4.2. The hybrid smoothed finite element method for acoustic problems

As mentioned in the published literature [39], the HS-FEM combines The NS-FEM and the standard FEM by introducing a scaled factor $\alpha \in [0, 1]$. In this paper, the problem domain is discretized into three-node triangular elements and the linear FEM shape functions are used. As presented in previous section, in the NS-FEM model each triangular elements in the problems domain will be divided into three quadrilateral sub-domains of equal area by connecting the centroids and mid-edge-point of the triangular elements and each sub-domain contributes to the element stiffness matrix of the node attached. While in the HS-FEM model, as shown in Fig. 4, the difference is that the three original quadrilateral sub-domains at the corners are scaled down by $(1-\alpha^2)$ with the help of a parameter α. As a result, the three quadrilateral sub-domains associated with three vertexes have an equal area of $(1-\alpha^2)A_e/3$ and the remaining Y-shaped sub-domain in the middle of the element has an area of $\alpha^2 A_e$, where A_e is the area of the triangular element.

Then the NS-FEM scheme is used to calculate the contributions to the element stiffness matrix of the three quadrilateral sub-domains and the standard FEM is used to calculate the contributions to the element stiffness matrix of the Y-shaped sub-domain. The global stiffness matrix in HS-FEM can be expressed as:

$$\overline{\mathbf{K}}^{\text{HS-FEM}} = \sum_{k=1}^{N_n}\overline{\mathbf{K}}_k^{\text{NS-FEM}} + \sum_{i=1}^{N_e}\overline{\mathbf{K}}_i^{\text{FEM}} \tag{32}$$

where

$$\overline{\mathbf{K}}_k^{\text{NS-FEM}} = \int_{\Omega_{k,\alpha}^s}(\overline{\mathbf{B}}^\alpha)^T\overline{\mathbf{B}}^\alpha\mathrm{d}\Omega \tag{33}$$

$$\overline{\mathbf{K}}_i^{\text{FEM}} = \int_{\Omega_{k,\alpha}^e}\mathbf{B}^T\mathbf{B}d\Omega = \mathbf{B}^T\mathbf{B}\alpha^2 A_i^e \tag{34}$$

where $\Omega_{k,\alpha}^s$ is the smoothing domain consist of three quadrilateral sub-domains and bounded by $\Gamma_{k,\alpha}^e$, as shown in Fig. 5. $\Omega_{k,\alpha}^e$ is the remaining Y-shaped sub-domain in the original triangular element.

Actually, the smoothed gradient field in the smoothing domain can be calculated as:

$$\overline{\mathbf{B}}^\alpha(\mathbf{x}_k) = \frac{1}{A_{k,\alpha}}\sum_{j=1}^{n_k^e}\frac{1}{3}(1-\alpha^2)A_j^e\mathbf{B}(\mathbf{x}_k) = \frac{1}{A_k^s}\sum_{j=1}^{n_k^e}\frac{1}{3}A_j^e\mathbf{B}(\mathbf{x}_k) = \overline{\mathbf{B}}(\mathbf{x}_k) \tag{35}$$

where $A_{k,\alpha}$ is the area of the domain $\Omega_{k,\alpha}^s$ and A_k^s is the area defined in Eq. (31), n_k^e is the number of elements around node k and A_j^e is the whole area of the jth element around node k.

Eq. (35) implies that $\overline{\mathbf{B}}^\alpha$ Eq. (33) can be replaced by $\overline{\mathbf{B}}(\mathbf{x}_k)$ in Eq. (28), and then Eq. (33) can be rewritten as

$$\overline{\mathbf{K}}_k^{\text{NS-FEM}} = (1-\alpha^2)\overline{\mathbf{B}}^T\overline{\mathbf{B}}A_k^s \tag{36}$$

Eqs. (34) and (36) show that the procedure of the HS-FEM is very simple and can be implemented in a straightforward way with little change to the original NS-FEM and FEM code.

5. Numerical error estimates in acoustic problems

It is well known that the quality of the numerical solution for acoustic problems using FEM depends on wave numbers k as well as the average mesh size h of the numerical model. For practical applications, acoustic finite element users usually follow the so-called "the rule of thumb" to obtain acceptable solution. According to "the rule of thumb", a wave-length should always be resolved by a constant number of elements. However, this rule can only provide reliable results in the low frequency range. For high frequency

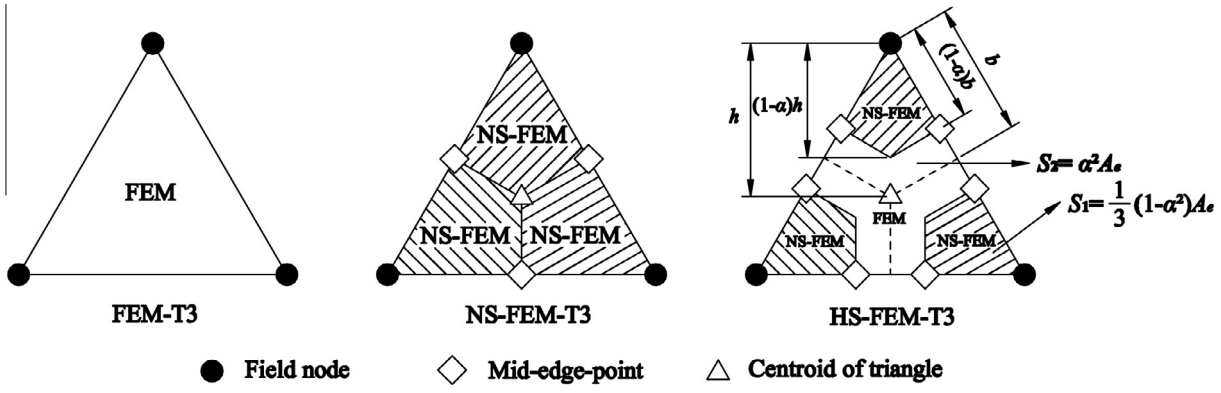

Fig. 4. The HS-FEM-T3 elements are formulated by combining FEM-T3 elements and NS-FEM-T3 elements: the NS-FEM is used for three quadrilateral smoothing domains and FEM is used for the remaining Y-shaped area.

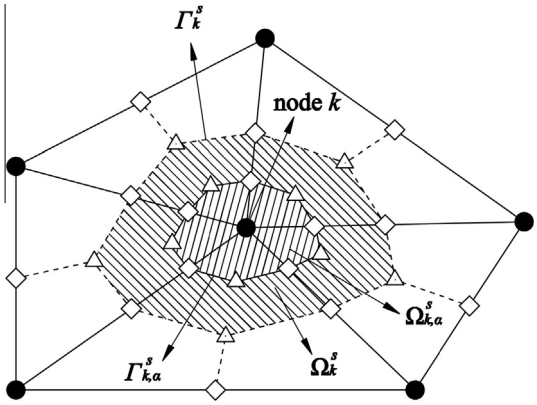

Fig. 5. Node-based smoothing domain associated with nodes in the HS-FEM model.

range, it cannot work well and the numerical error may be prohibitive.

As the published literature mentioned [40], the numerical discretization error in the H^1-semi-norm can be expressed as:

$$|p^e - p^h|^2 = \int_\Omega (\tilde{v}^e - \tilde{v}^h)^T (v^e - v^h) d\Omega \tag{37}$$

where $\tilde{v}$ is the complex conjugate of the velocity, the superscript e denotes the exact solutions and h denotes the numerical solutions obtained from numerical methods including the present HS-FEM and standard FEM.

Ihlenburg and Babuška [40] proved that the relative error of the hp-version FEM solution for acoustic problem in H^1-seminorm is bounded by

$$\eta = \frac{|p^e - p^h|_1}{|p^e|_1} = \sqrt{\frac{\int_\Omega (\tilde{v}^e - \tilde{v}^h)^T (v^e - v^h) d\Omega}{\int_\Omega (\tilde{v}^e \cdot v^e)^2 d\Omega}} \leqslant C_1 \left(\frac{kh}{p}\right)^p + C_2 k \left(\frac{kh}{p}\right)^{2p} \tag{38}$$

where p is the degree of polynomial approximation used in the numerical methods.

Ihlenburg and Babuška [40] proved that the numerical error can be split into two terms: the first term in Eq. (38) denotes the interpolation error. This error can be controlled by keeping kh constant. The second term denotes the numerical pollution error caused not only by phase shift but also the error on the amplitude of the wave.

For linear interpolation ($p = 1$) discussed in this paper, the pollution error term can be neglected if $kh < 1$, so the relative error is mainly caused by the interpolation error term for small wave numbers. While for large wave numbers, the pollution error term will dominates the relative error, because it will increase linearly with the increase of wave number k.

In this present paper, the relative error of the numerical solution obtained from the standard FEM and HS-FEM will be discussed in details. The numerical results demonstrate that the numerical error will reduce significantly due to the gradient smoothing operation on the numerical model and the HS-FEM can obtain more accurate results than the standard FEM.

6. Numerical results

In this section, a number of numerical examples are conducted to verify the improved accuracy of the present HS-FEM. For acoustic problems, we have known that the wave number solution of FEM is always smaller than the exact solution due to the "overly-stiff" property of the model and the NS-FEM solution is always larger than the exact one due to the "overly-soft" property, so the value of the important parameter α, which controls the contribution proportions of the FEM and NS-FEM to the present HS-FEM model, is very critical in improving the accuracy of the numerical results. The optimal α, which can provide nearly exact stiffness of the model, not only depends on the wave number but also on the mesh size and the wave propagation angle in two dimensional acoustic problems, and therefore a universally workable α is not easy to find. Interested readers may refer to the published work [41] on how to determine the optimal value of α in 1D and 2D acoustic problems. The aim of this paper is to solve two dimensional acoustic radiation problems with more accurate results using the HS-FEM and extending the application of the HS-FEM from interior acoustic problems in bounded domains to exterior acoustic problems in unbounded domains. For simplicity, the value of the parameter α is chosen to be 0.8 for all numerical examples except for extra instruction in this paper. This value of α is found preferable by numerical "experiments" on different meshes. This α chosen will not be optimal and the solution may not be very close to the exact one, but the accuracy of the results is usually much better than the FEM using the same mesh.

6.1. Acoustic radiation from an infinite oscillating cylinder

6.1.1. Accuracy study

An infinite rigid oscillating cylinder of order n is considered in this section, Fig. 6a shows the geometry of the cylinder. The cylinder of radius a is located in the unbounded domain. The density of the medium is 1000 kg/m^3 and the speed of the wave is 1500 m/s. Because one of the dimensions is quite larger than the two other ones, this three-dimensional problems can be simplified as a general two dimensional problems. The numerical model of this

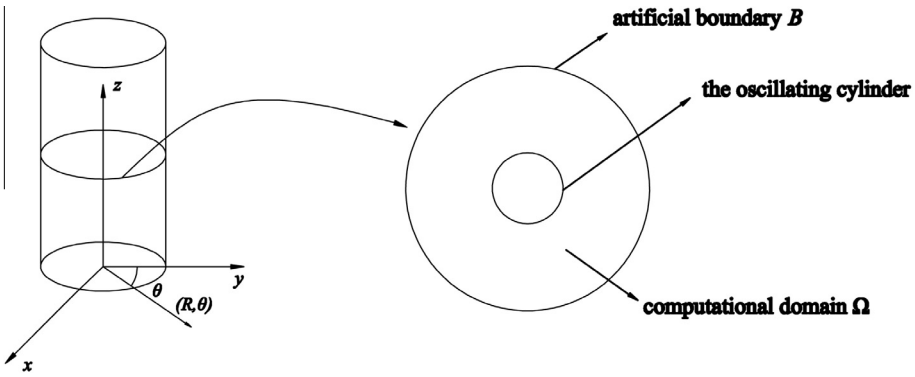

Fig. 6a. Schematic description of the oscillating cylinder of order n located in the infinite domain.

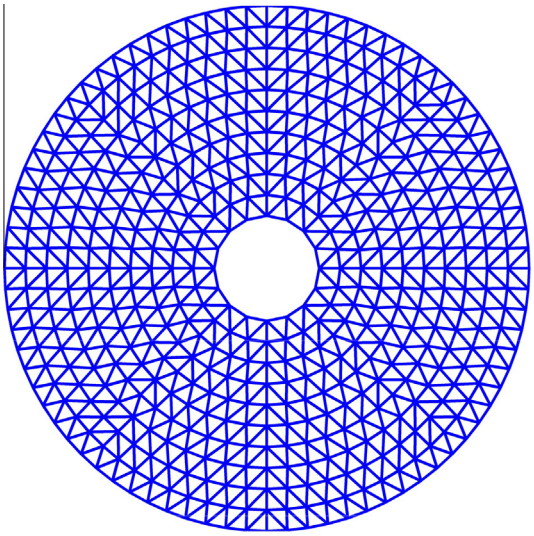

Fig. 6b. The numerical model of the acoustic radiation problem.

problem is shown in Fig. 6b. The center of the cylinder is located at (0, 0) and the artificial boundary B with the center at (0, 0) is a circle of radius $R = 1$. The analytical solution to this acoustic radiation problem is given by:

$$p = \frac{H_n(kr)\cos n\theta}{H_n(ka)} \tag{39}$$

where H_n is Hankel function of the first kind of order n and k is the wave number.

For the purpose of testing the performance of the proposed method, for mode $n = 2$, three different geometrically non-dimensionalized wave numbers ($ka = 0.2\pi$, 0.4π, 0.6π) are employed to compute the acoustic pressure distribution along the artificial boundary using HS-FEM with average mesh size of 0.08 m. The imaginary part of acoustic pressure along the artificial boundary as a function of the polar angle is plotted in Fig. 7. For the purpose of comparison, the numerical results obtained from the standard FEM and HS-FEM with the same mesh together with the analytical solutions are presented in the figures. It can be seen from the figures that both FEM and HS-FEM can provide reliable results which agree well with the exact solution at small wave numbers, while at large wave numbers, the numerical results obtained from FEM may depart from the exact solution, the results of HS-FEM are still in good agreement with the exact one. This numerical example demonstrates that HS-FEM can provide very properly softened stiffness of the numerical model and can achieve more accurate results than the FEM.

Furthermore, for mode $n = 3$, the directivity patterns of the radiated acoustic pressure with different geometrically non-dimensionalized wave numbers ($ka = 0.1\pi$, 0.3π, 0.5π, 0.7π) are also considered. The HS-FEM results in comparison to the FEM results and analytical solutions are depicted in Fig. 8. From the results, it can be seen that both HS-FEM and FEM results are in good agreement with the analytical solutions for small wave numbers. When it comes to large wave numbers, the results from HS-FEM will stand out and are more accurate than those from FEM. This again verifies that HS-FEM performs better than FEM and can achieve more accurate results for acoustic radiation problems, especially for large wave numbers.

6.1.2. Convergence study

This section will investigate the convergence rate of the present HS-FEM for acoustic radiation problems by employing several different meshes. Fig. 9 depicts the relative error as a function of the average mesh size at different wave number of $k = 3\pi$ and $k = 6\pi$ for both HS-FEM and FEM results. It can be found from the figure that: for small wave number ($k = 3\pi$), the relative error of both HS-FEM and FEM are about 10%, while the results of present HS-FEM are more accurate than that of FEM results. Besides, the results of HS-FEM converge faster than that of FEM do when the mesh gets finer. For large wave number ($k = 6\pi$), the relative error

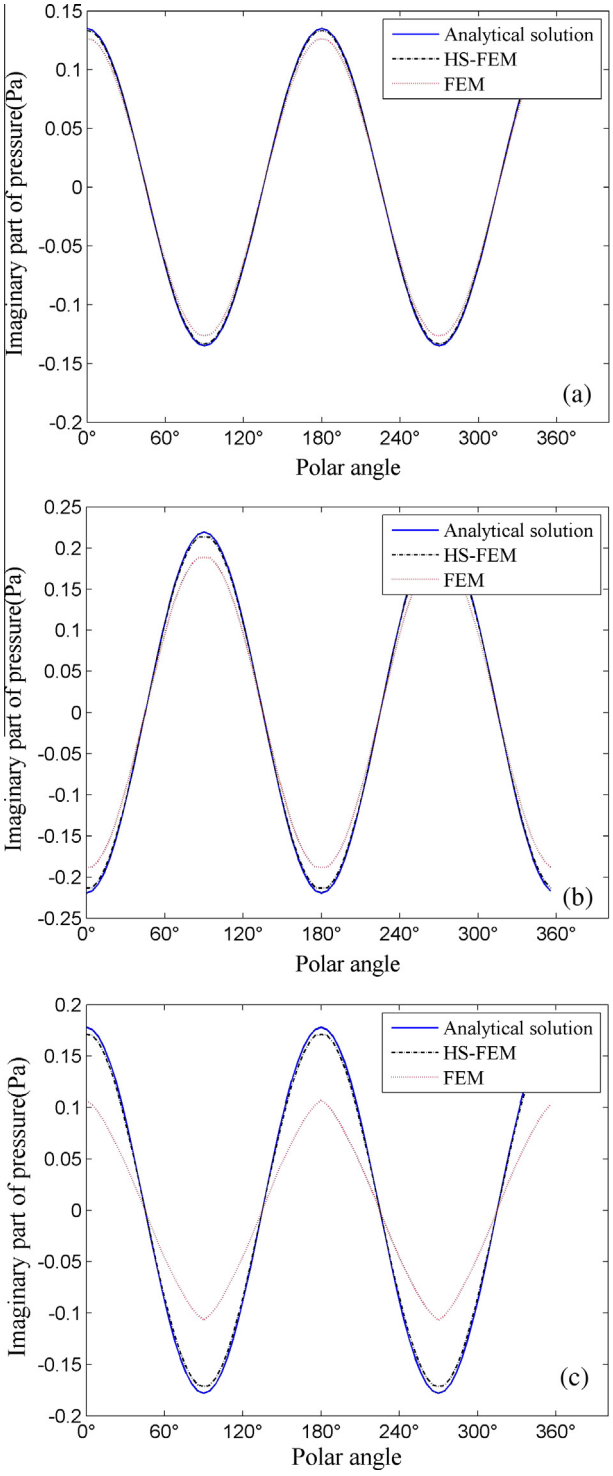

Fig. 7. The imaginary part of pressure as a function of the polar angle along the artificial boundary at different geometrically non-dimensionalized wave numbers: (a) $ka = 0.2\pi$; (b) $ka = 0.4\pi$; (c) $ka = 0.6\pi$.

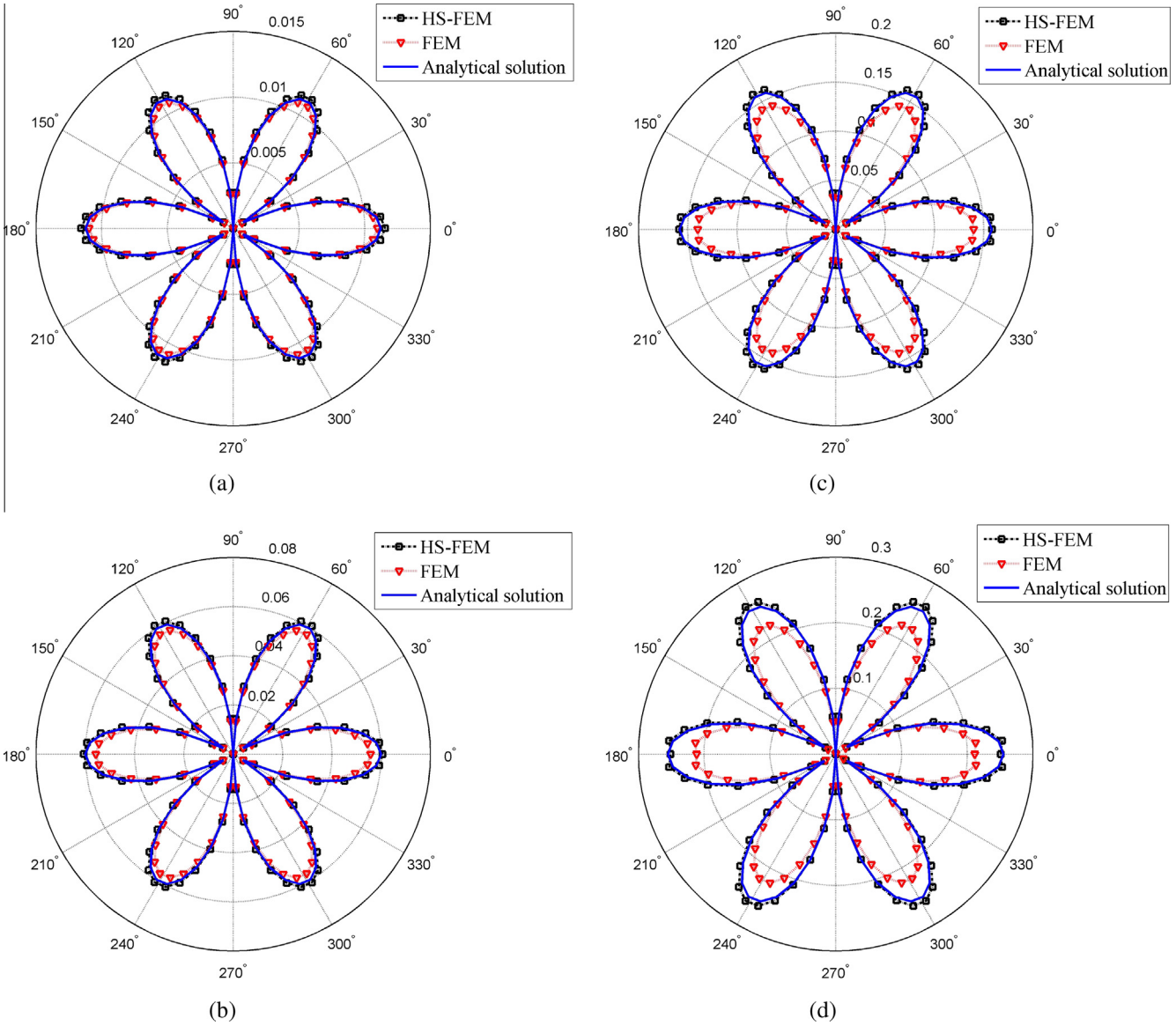

Fig. 8. The directivity patterns of the radiated acoustic pressure with different geometrically non-dimensionalized wave numbers: (a) $ka = 0.1\pi$; (b) $ka = 0.3\pi$;(c) $ka = 0.5\pi$; (d) $ka = 0.7\pi$.

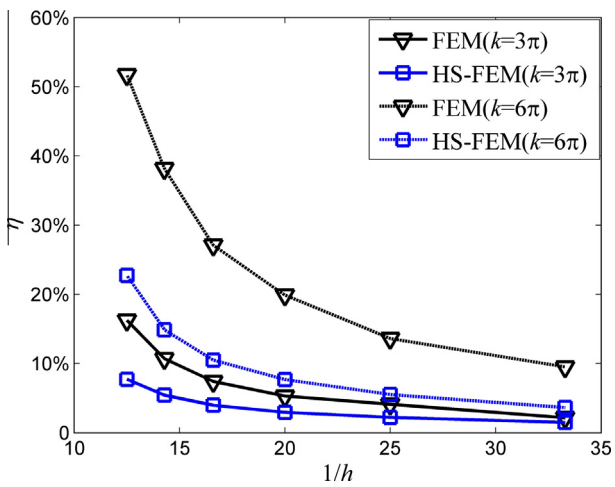

Fig. 9. Comparison of convergence rate of the results from HS-FEM and FEM with different meshes.

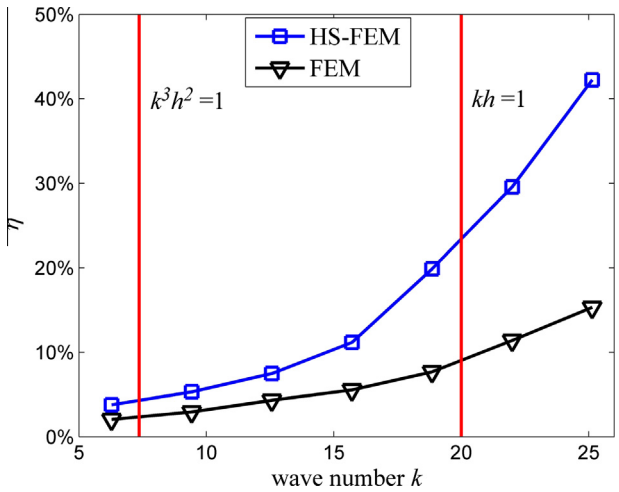

Fig. 10. The relative error in the H^1 semi-norm against the wave number k for both HS-FEM and FEM solutions.

of both HS-FEM and FEM will increase significantly, compared to FEM, the HS-FEM solutions is obviously better. These findings show that HS-FEM works very well and converges much faster than FEM.

6.1.3. Control of the numerical error

Eq. (38) shows the upper bound of the relative error in H^1 semi-norm for the method of *hp* version. For linear elements ($p = 1$) used in this paper, the relative error is bounded by:

$$\eta = \frac{|p^e - p^h|_1}{|p^e|_1} = \sqrt{\frac{\int_\Omega (\tilde{v}^e - \tilde{v}^h)^T (v^e - v^h) d\Omega}{\int_\Omega (\tilde{v}^e \cdot v^e)^2 d\Omega}} \leqslant C_1 kh + C_2 k^3 h^2 \tag{40}$$

Eq. (40) means that the control of the relative error requires considering both kh and k^3h^2. Fig. 10 shows the relative error against the wave number k for both HS-FEM and FEM solutions.

For the purpose of discuss, cases of $kh = 1$ (the interpolation error) and $k^3h^2 = 1$ (the pollution error) are also plotted in the figure. It can be observed from the figure that the relative error obtained from HS-FEM and FEM are both very small for low wave numbers. However, the relative errors increase quickly as the wave number k grows, while HS-FEM performs better than the FEM and can achieve more accurate results for the full wave number range.

Furthermore, in order to study the control of numerical error with the present method clearly. The relative errors are computed on a range of different meshes by keeping $kh = cst$ and $k^3h^2 = cst$. Fig. 11 shows the relative error against $1/h$ with varying h and keeping kh constant using HS-FEM and FEM. From the results in Fig. 11, it can be found that: for small wave number range, the interpolation error (the first term in Eq. (40)) is well controlled if kh is kept constant for both HS-FEM and FEM; for large wave number range, the upper bound of the relative error of FEM results will increase dramatically. It means that the pollution error will dominate the relative error because the pollution error (the second term in Eq. (40)) will increase linearly with wave number $k = 1/h$. While the HS-FEM results do not deteriorate significantly with the increase of k. This means that a certain level of relative error can be controlled by the gradient smoothing techniques used in the HS-FEM. Fig. 12 shows the relative error against $1/h$ with varying h and keeping k^3h^2 constant. From the results in Fig. 12, the upper bound of relative error is well controlled for both HS-FEM and FEM k^3h^2 is kept constant. This is because not only the interpolation error but also the pollution error can be controlled in the case $k^3h^2 = cst$ based on Eq. (40). Compared to FEM, the HS-FEM still provide more stable results.

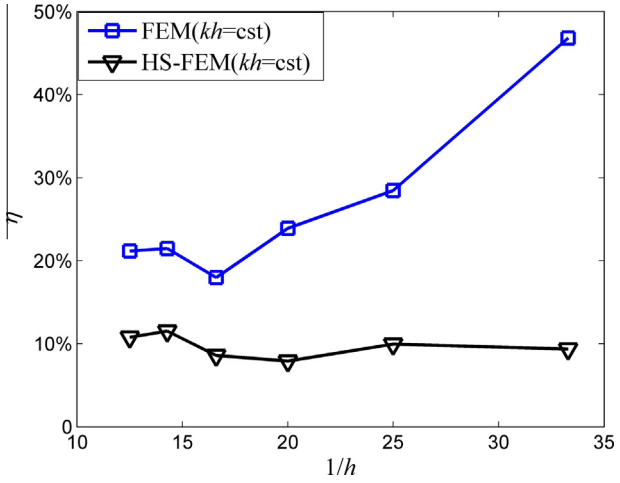

Fig. 11. Evolution of the relative error in H^1 semi-norm as a function of $1/h$ with varying h and keeping kh constant.

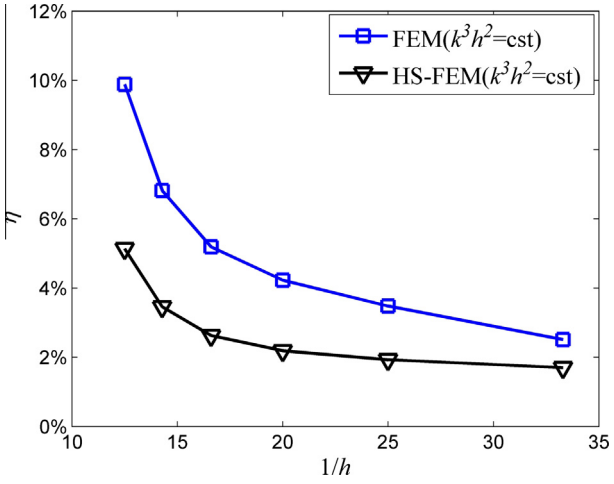

Fig. 12. Evolution of the relative error in H^1 semi-norm as a function of $1/h$ with varying h and keeping k^3h^2 constant.

6.2. An arbitrary shaped radiator

In this example, as shown in Fig. 13, a realistic acoustic radiation problem of an arbitrary shaped radiator is investigated to demonstrate the property of the proposed HS-FEM. The Neumann boundary condition with $v_n = 10^{-4}$ m/s is imposed on the surface of the radiator. The artificial boundary B is still a circle of radius $R = 1$ with the center at (0, 0) and the parameters of the fluid medium are the same as the problem discussed in the previous section. The computational domain consists of 1548 nodes and 2948 triangular elements. The real part of the acoustic pressure on the artificial boundary as a function of the polar angle are plotted in Fig. 14. Since the analytical solution for this problem is unavailable, a reference results obtained using FEM with a very fine mesh are also presented in the figures for comparison. From the figures, it can be found that the scatter acoustic pressure distribution obtained from HS-FEM are very close to the reference results in both large and small wave numbers. While the corresponding results obtained from FEM depart from the reference results a lot when the wave numbers get large. This numerical example again indicates that the HS-FEM perform much better and can give much more accurate results than FEM for acoustic scattering problems.

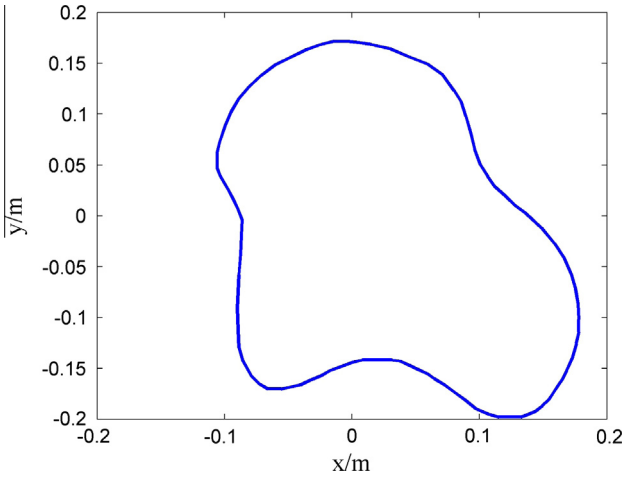

Fig. 13. The acoustic radiation problem with a irregular radiator.

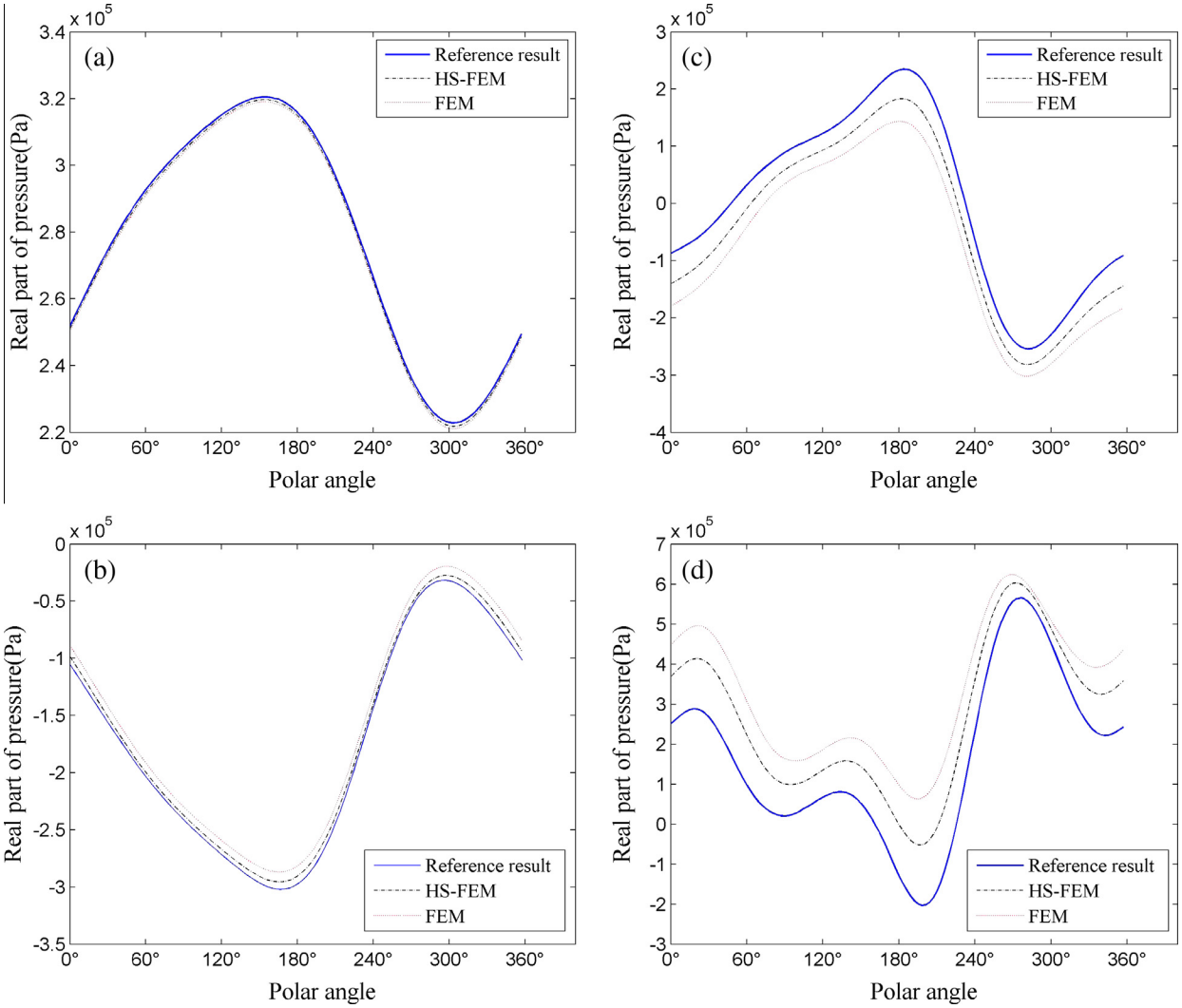

Fig. 14. The real part of the acoustic pressure as a function of the polar angle along the artificial boundary at different wave numbers for the irregular radiator: (a) $k = \pi$; (b) $k = 2\pi$; (c) $k = 3\pi$; (d) $k = 4\pi$.

6.3. 2D car acoustic radiation problems

In this section, a two-dimensional steady-state acoustic radiation problem of 2D car is considered. As shown in Fig. 15, assuming the shape of the car is prismatic, and then this 3D problem can be simplified to 2D. Note that the exterior radiated noise of car body is mainly from the vibration of engine, only the front panel and hood of engine is subjected to a vibration velocity of 10^{-3} m/s. The material parameters are taken as air density $\rho = 1.225$ kg/m^3 and sound speed $c = 340$ m/s. In order to obtain the finite computational domain, the infinite domain is truncated by the artificial boundary, which is still a circle, and the observation point A is on the circle

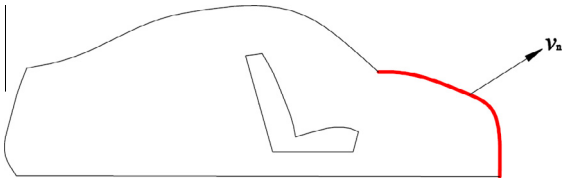

Fig. 15a. The geometry of the 2D car.

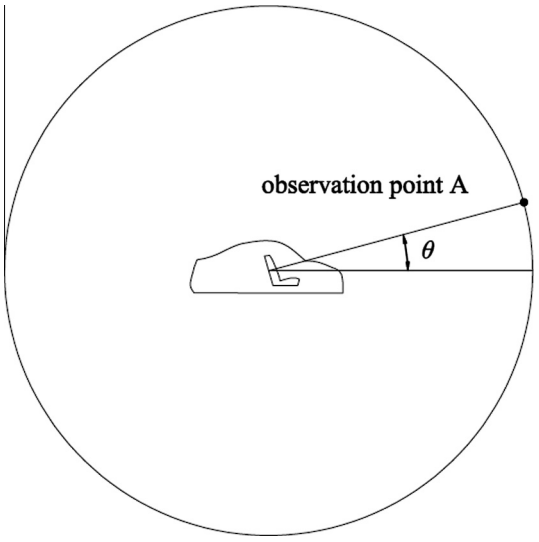

Fig. 15b. The numerical model of the acoustic radiation problems of 2D car.

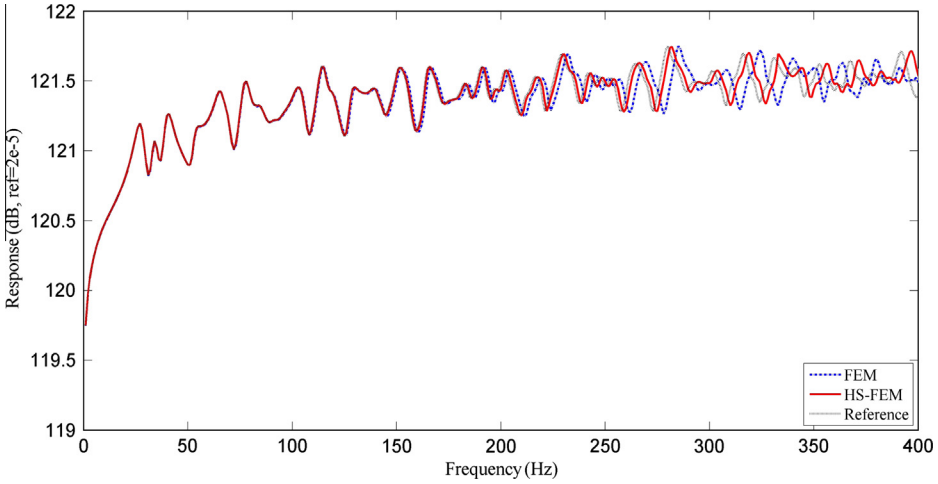

Fig. 16. The frequency response at observe point obtained from FEM and HS-FEM.

with angle $\theta = 15$. The discretized numerical model consists of 3804 nodes and 7352 triangular elements with an average mesh size of 0.1 m. The frequency response analysis at observe point is conducted to study the acoustic distribution of this problem. Fig. 16 shows the numerical results obtained from FEM and present HS-FEM. The frequency range is chosen from 1 Hz to 400 Hz and the interval is 1 Hz. Note that there is no analytical solution to this problem, the FEM solution with a very fine mesh (11,788 nodes and 23,139 triangular elements) is also presented as a reference for comparison. From the figure, it is found that both FEM and present HS-FEM solutions agree well with the reference solution in the low frequency range. With the increase of the frequency, the results from FEM may be unreliable, while the present HS-FEM can still provide very accurate results. This practical numerical example again demonstrates that the HS-FEM performs better and can achieve much more accurate results than FEM for two-dimensional radiation problems, especially for high frequency range.

7. Conclusions

In this paper, the hybrid smoothed finite element (HS-FEM) is combined with the well-known Dirichlet-to-Neumann (DtN) boundary condition to give a HS-FEM-DtN model for two dimensional acoustic radiation problems. Through the formulations and the numerical results, several major concluding remarks can be drawn as follows:

(1) Coupling of the HS-FEM and the well known DtN boundary condition works well for two dimensional acoustic radiation problems and can provide very stable numerical results.
(2) The HS-FEM is equipped a scaling factor α that controls the contributions from the node-based smoothed finite element method (NS-FEM) and standard FEM. This novel combination makes the best use of the "overly-soft" property of the NS-FEM and the "overly-stiff" property of the standard FEM. Therefore the HS-FEM is capable to provide a "nearly exact" solution with very coarse meshes.
(3) For the two dimensional acoustic radiation problems discussed in this paper, the implementation of the HS-FEM is very easy since no additional parameters and degrees of freedom are needed, hence it can be implemented from the original FEM code with little modification.
(4) For the practical acoustic radiation problems with complicated geometry, the HS-FEM performs better than the FEM with the same mesh. It indicates that the HS-FEM is capable to solve the real engineering problems with very accurate results.

References

[1] Crocker MJ. Prediction of transmission loss in mufflers by the finite–element method. J Acoust Soc Am 1975;57(1):144–8.
[2] Petyt M, Lea J, Koopmann GH. A finite element method for determining the acoustic modes of irregular shaped cavities. J Sound Vib 1976;45(4):495–502.
[3] Nefske DJ, Wolf JA, Howell LJ. Structural-acoustic finite element analysis of the automobile passenger compartment: a review of current practice. J Sound Vib 1982;80(2):247–66.
[4] Harari I, Magoulès F. Numerical investigations of stabilized finite element computations for acoustics. Wave Motion 2004;39(4):339–49.
[5] Assaad J, Decarpigny JN, Bruneel C, Bossut R, Hamonic B. Application of the finite element method to two-dimensional radiation problems. J Acoust Soc Am 1993;94(1):562–73.
[6] Ihlenburg F, Babuška I. Finite element solution of the Helmholtz equation with high wave number Part I: the h-version of the FEM. Comput Math Appl 1995;30(9):9–37.
[7] Ihlenburg F, Babuska I. Finite element solution of the Helmholtz equation with high wave number Part II: the hp version of the FEM. SIAM J Numer Anal 1997;34(1):315–58.
[8] Deraemaeker A, Babuška I, Bouillard P. Dispersion and pollution of the FEM solution for the Helmholtz equation in one, two and three dimensions. Int J Numer Methods Eng 1999;46(4):471–99.
[9] Higdon RL. Absorbing boundary conditions for elastic waves. Geophysics 1991;56(2):231–41.
[10] Clayton R, Engquist B. Absorbing boundary conditions for acoustic and elastic wave equations. Bull Seismol Soc Am 1977;67(6):1529–40.
[11] Higdon RL. Numerical absorbing boundary conditions for the wave equation. Math Comput 1987;49(179):65–90.
[12] Hu FQ. Absorbing boundary conditions. Int J Comput Fluid D 2004;18 (6):513–22.
[13] Keller JB, Givoli D. Exact non-reflecting boundary conditions. J Comput Phys 1989;82(1):172–92.
[14] Harari I, Patlashenko I, Givoli D. Dirichlet-to-Neumann maps for unbounded wave guides. J Comput Phys 1998;143(1):200–23.
[15] Grote MJ, Kirsch C. Dirichlet-to-Neumann boundary conditions for multiple scattering problems. J Comput Phys 2004;201(2):630–50.
[16] Giljohann D, Bittner M. The three-dimensional DtN finite element method for radiation problems of the Helmholtz equation. J Sound Vib 1998;212 (3):383–94.
[17] Givoli D, Patlashenko I, Keller JB. Discrete Dirichlet-to-Neumann maps for unbounded domains. Comput Methods Appl Mech Eng 1998;164(1):173–85.
[18] Hastings FD, Schneider JB, Broschat SL. Application of the perfectly matched layer (PML) absorbing boundary condition to elastic wave propagation. J Acoust Soc Am 1996;100(5):3061–9.
[19] Berenger JP. A perfectly matched layer for the absorption of electromagnetic waves. J Comput Phys 1994;114(2):185–200.

[20] Turkel E, Yefet A. Absorbing PML boundary layers for wave-like equations. Appl Numer Math 1998;27(4):533–57.
[21] Acosta S, Villamizar V. Coupling of Dirichlet-to-Neumann boundary condition and finite difference methods in curvilinear coordinates for multiple scattering. J Comput Phys 2010;229(15):5498–517.
[22] Acosta S, Villamizar V, Malone B. The DtN nonreflecting boundary condition for multiple scattering problems in the half-plane. Comput Methods Appl Mech Eng 2012;217:1–11.
[23] Nicholls DP, Nigam N. Exact non-reflecting boundary conditions on general domains. J Comput Phys 2004;194(1):278–303.
[24] Thompson LL, Pinsky PM. A Galerkin least-squares finite element method for the two-dimensional Helmholtz equation. Int J Numer Methods Eng 1995;38 (3):371–97.
[25] Franca LP, Farhat C, Macedo AP, Lesoinne M. Residual-free bubbles for the Helmholtz equation. Int J Numer Methods Eng 1997;40(21):4003–9.
[26] Belytschko T, Lu YY, Gu L. Element-free Galerkin methods. Int J Numer Methods Eng 1994;37(2):229–56.
[27] Bouillard P, Suleaub S. Element-Free Galerkin solutions for Helmholtz problems: formulation and numerical assessment of the pollution effect. Comput Methods Appl Mech Eng 1998;162(1):317–35.
[28] Alvarez GB, Loula AFD, do Carmo EGD, Rochinha FA. A discontinuous finite element formulation for Helmholtz equation. Comput Methods Appl Mech Eng 2006;195(33):4018–35.
[29] He ZC, Liu GR, Zhong ZH, Wu SC, Zhang GY, Cheng AG. An edge-based smoothed finite element method (ES-FEM) for analyzing three-dimensional acoustic problems. Comput Methods Appl Mech Eng 2009;199 (1):20–33.
[30] Liu GR, Nguyen TT, Dai KY, Lam KY. Theoretical aspects of the smoothed finite element method (SFEM). Int J Numer Methods Eng 2007;71(8):902–30.
[31] Liu GR, Dai KY, Nguyen TT. A smoothed finite element method for mechanics problems. Comput Mech 2007;39(6):859–77.
[32] Li Y, Li M, Liu GR. A modified triangulation algorithm tailored for the smoothed finite element method (S-FEM). Int J Comput Methods 2014;11(01).
[33] Liu GR, Nguyen TT, Lam KY. An edge-based smoothed finite element method (ES-FEM) for static, free and forced vibration analyses of solids. J Sound Vib 2009;320(4):1100–30.
[34] He ZC, Cheng AG, Zhang GY, Zhong ZH, Liu GR. Dispersion error reduction for acoustic problems using the edge-based smoothed finite element method (ES-FEM). Int J Numer Methods Eng 2011;86(11):1322–38.
[35] He ZC, Li GY, Zhong ZH, Cheng AG, Zhang GY, Li E, et al. An ES-FEM for accurate analysis of 3D mid-frequency acoustics using tetrahedron mesh. Comput Struct 2012;106:125–34.
[36] He ZC, Liu GR, Zhong ZH, Cui XY, Zhang GY, Cheng AG. A coupled edge-/face-based smoothed finite element method for structural–acoustic problems. Appl Acoust 2010;71(10):955–64.
[37] He ZC, Liu GR, Zhong ZH, Zhang GY, Cheng AG. A coupled ES-FEM/BEM method for fluid–structure interaction problems. Eng Anal Bound Elem 2011;35 (1):140–7.
[38] Li W, Chai YB, Lei M, Liu GR. Analysis of coupled structural-acoustic problems based on the smoothed finite element method (S-FEM). Eng Anal Bound Elem 2014;42(1):84–91.
[39] Li E, He ZC, Xu X, Liu GR. Hybrid smoothed finite element method for acoustic problems. Comput Methods Appl Mech Eng 2015;283:664–88.
[40] Ihlenburg F, Babuška I. Reliability of finite element methods for the numerical computation of waves. Adv Eng Softw 1997;28:417–24.
[41] He ZC, Liu GR, Zhong ZH, Zhang GY, Cheng AG. Dispersion free analysis of acoustic problems using the alpha finite element method. Comput Mech 2010;46:867–81.